

# SEEPAGE-INDUCED SLOPE FAILURES ON SANDBARS IN GRAND CANYON

By Muniram Budhu,<sup>1</sup> Member, ASCE, and Roger Gobin<sup>2</sup>

**ABSTRACT:** The effect of fluctuating discharge from Glen Canyon Dam on downstream sandbars is of significant concern to dam operators, environmentalists, and the public. In this contribution, the observations of seepage-related erosion caused by fluctuations in dam discharge are presented. A finite-element model embracing Biot's coupled stress-pore water pressure theory is used to study seepage-induced slope failures of sandbars in the Grand Canyon. In addition, a simple model based on seepage parallel to slope in an infinite, homogeneous, cohesionless soil was used to determine the limiting stable seepage slope. In this paper, it is shown that this limiting stable seepage slope becomes a predefined failure plane. Sand deposited above this stable seepage slope will eventually fail along the predefined plane from gravitational forces, high pore-water pressure and seepage forces. Field data from an instrumented sandbar in the Grand Canyon subjected to the fluctuating discharge from Glen Canyon Dam are compared with the predictions from the simple model, the finite-element model, and conventional slope-stability analyses.

## INTRODUCTION

Glen Canyon Dam, located in the northeastern corner of Arizona (Fig. 1), was commissioned in 1963 to provide flood control, water storage, and hydroelectric power for some western states in the United States. The dam is a "peaking facility," which means that it is operated to satisfy peak electrical-power demands that usually occur around the middle of the day. Discharge from the dam fluctuates, creating a daily tide in the Colorado River downstream of the dam. Typical daily river stage fluctuation is between 1 and 3 m, with some narrow river sections reaching 4 m.

Sandbars are scattered along the banks of the main channel but are more prevalent at the confluences of ephemeral tributaries and the main channel (Schmidt and Graf 1990). During floods or high dam releases, deposits at the confluences and fresh sediments from the ephemeral tributaries are transported and then redeposited to form new sandbars or enlarge existing sandbars. The sandbars provide a natural environment for riparian habitat. Campers and hikers use some sandbars as campsites; these are often referred to as beaches.

In the predam era, the mean annual maximum flow was 2,439 m<sup>3</sup>/s, with a record flow of 5,660 m<sup>3</sup>/s in 1921 (Schmidt and Graf 1990). Maximum flows usually occurred during the spring snowmelt and caused scouring on some sandbars. However, after the floodwaters receded, some scoured areas were subsequently rebuilt.

Glen Canyon Dam now regulates the flow of Colorado River in response to electrical demands. The range of discharge varies daily and seasonally. However, flows usually fluctuate within the range of 57 to 849 m<sup>3</sup>/s. There are public concerns that the fluctuating discharge from Glen Canyon Dam is responsible for the erosion of sandbars and the concomitant loss of the postdam ecology and recreational facilities.

During a study period from June 1990 to July 1991, Colorado River downstream of Glen Canyon Dam was occasionally used as an experimental flume. Some observations of seepage erosion due to transient dam discharge during the experimental flows are presented and two analyses are pro-

posed—a simple analysis and a finite-element analysis—for slope failures (bank cuts, mass wasting) resulting from transient ground-water seepage.

## BACKGROUND AND DESCRIPTION OF TEST PROGRAM FOR SEEPAGE EROSION STUDIES

Several sandbar sites along Colorado River downstream of the dam were selected for detailed studies during the experimental flow period. Three sandbars (test sites), -6.5R, 43L, and 172L (Fig. 1), were instrumented with a network of pore-water-pressure sensors, temperature sensors, and tiltmeters (Carpenter et al. 1992). Rainfall and other hydrologic measurements, bathymetry, aerial photography, and time-lapsed photography were part of the instrumentation and measurement package adopted to monitor the test sites. Ground sur-

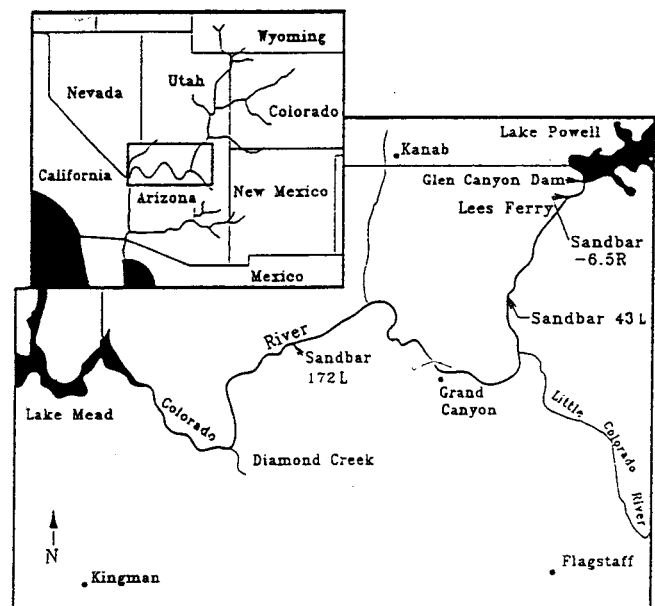


FIG. 1. Study Area

TABLE 1. Soil Properties Used in Finite-Element Analysis

Soil Parameters			Zone I	Zone II
(1)	(2)	(3)	(4)	(5)
Shear modulus	$G$	kPa	3,700	3,500
Permeability	$k$	cm/s	$2.3 \times 10^{-2}$	$4.2 \times 10^{-2}$
Angle of friction	$\phi$	degrees	32	30
Cohesion	$c$	kPa	2.0	4.0
Saturated unit weight	$\gamma_{sat}$	kN/m <sup>3</sup>	17.2	16.0

<sup>1</sup>Assoc. Prof., Dept. of Civ. Engrg. and Engrg. Mech., Univ. of Arizona, Tucson, AZ 85721.

<sup>2</sup>Grad. Student, Dept. of Civ. Engrg. and Engrg. Mech., Univ. of Arizona, Tucson, AZ.

Note. Discussion open until January 1, 1996. To extend the closing date one month, a written request must be filed with the ASCE Manager of Journals. The manuscript for this paper was submitted for review and possible publication on August 8, 1994. This paper is part of the *Journal of Geotechnical Engineering*, Vol. 121, No. 8, August, 1995. ©ASCE, ISSN 0733-9410/95/0008-0601-0609/\$2.00 + \$.25 per page. Paper No. 9020.

veys were conducted before and soon after each research flow. Soil properties (Table 1) at each site were characterized by field and laboratory tests.

### OBSERVED SEEPAGE EROSION

Three agents of erosion were observed to be responsible for the current erosion of sandbars along Colorado River below Glen Canyon Dam: (1) Tractive forces; (2) wave action; and (3) seepage. Seepage erosion is the most ubiquitous agent of erosion (Budhu 1992; Budhu and Gobin 1994, 1995; Werell et al. 1992) and is the subject of this paper.

Seepage erosion induces many different types of geomorphic changes, described by several terms in the literature such as artesian sapping, spring sapping, seepage-driven erosion, rilling, tunnel scour, mass wasting, seepage-induced transport, and seepage weathering. Howard and McLane (1988) summarized many early observations relating to these terms, and theories concerning the geomorphical changes in riverbanks. We use the term "seepage erosion" to describe slope failures (also called mass wasting or bank cuts) resulting from transient seepage of ground water. Several seepage related erosion features were observed in many sandbars downstream of Glen Canyon Dam. Two of the predominant features are presented here.

When power demands are to be met, water is released through the turbines and the river stage rises. Water infiltrates the sandbars and the ground-water level rises. When power demands are met, some penstocks are closed, the river stage falls, and the volume of water stored within the banks during the rising stage must drain. Usually, the river stage falls faster than the rate of drainage of the stored ground water and thus a seepage face develops between the river level and the exit elevation of the ground water. The exit hydraulic gradient ( $i$ ) for many sandbars is sufficiently large to cause static liquefaction of the soil. Static liquefaction in this context means the transformation of a soil from a solid-like material to a viscous-like fluid. The soil is then carried in suspension by the outflow of water. Rivulets and gullies (rilling process) are formed below the exit point along the sandbar as the bank-stored water with its sediments flows down slope toward the river. These rivulets and gullies are scoured deeper as the water picks up sediments along its path to the river. A typical example of this seepage erosion feature is shown in Fig. 2. This type of erosion is prevalent on sandbars with slopes of less than  $15^\circ$ .

The upramping rate (the rate of dam discharge when electrical power demands are increasing) and the downramping rate (the rate of dam discharge when electrical power demands are reducing) are not constant. At high downramping rate ( $>50 \text{ m}^3/\text{s}/\text{hr}$ ), the elevated pore-water pressures and seepage stresses reduce the shear strength of the soil leading to slope failures. This condition is not a true undrained failure condition as is often assumed for rapid drawdown in reservoirs. A typical example of this type of seepage induced failure is shown in Fig. 3. Slope failures are catastrophic and often involve a large portion of the sandbar face. A substantial area of the sandbar can be lost in a few seconds. This type of failure usually occurs at the low-river stage and especially on weekends, when electrical-power demands and, consequently, the river stage are at their lowest level.

On occasions, incipient slope failures (failure plane is visible but the soil mass does not collapse) may occur during falling river stage. Failure is then observed on the next rising river stage. It is quite easy to confuse this seepage-related failure with a tractive-force-induced failure. The dam operation practice of rapid downramping followed by a constant low stage over a day or more provokes these failures.

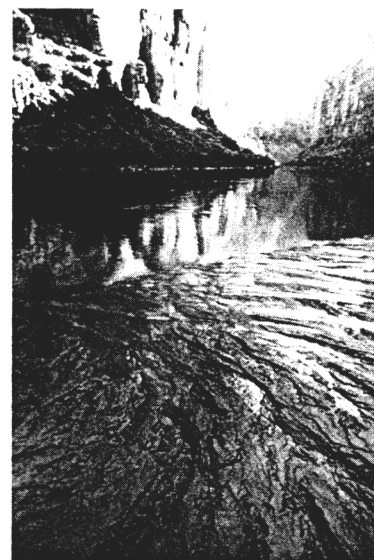


FIG. 2. Rivulets and Gullies Formed by Rilling



FIG. 3. Slope Failure due to Ground-Water Seepage at Left End of Sandbar

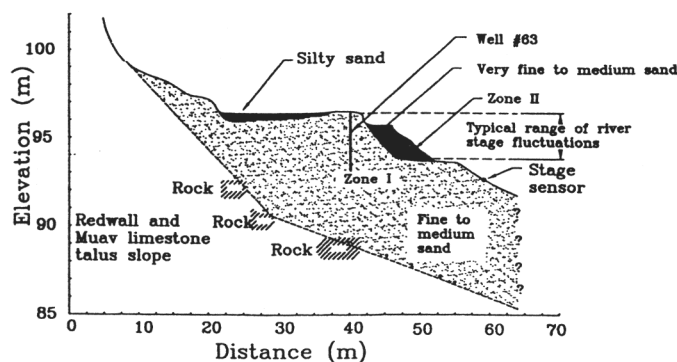


FIG. 4. Geological Section of Sandbar 172L

### SEEPAGE EROSION ON SANDBAR 172L

Sandbar 172L is located 277 km (172 mi) downstream of Lees Ferry, on the left bank of the Colorado River, in Grand Canyon National Park (Fig. 1). This sandbar was selected because it is the most dynamic of the three test sites. It underwent several cycles of erosion and deposition during the study period. Sandbar 172L is composed of two zones of material (Fig. 4). Zone I, a stable zone, is composed of fine to medium sand with a small amount of silt ( $<10\%$  by weight). Zone II, an unstable zone of varying size, is composed of very fine to medium sand with a small amount of silt and clay. A summary of the material properties of zones I and II is shown in Table 1.

We now describe a particular event and use this event to

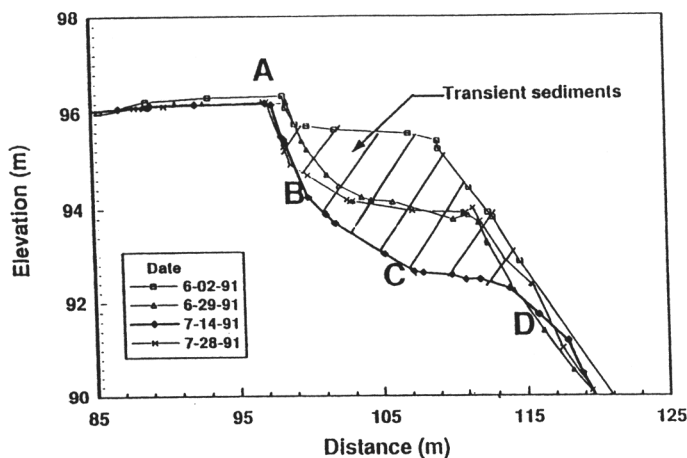


FIG. 5. Typical Changes in Geometry of Sandbar 172L as Determined from Ground Surveys

test the predictions from two proposed models and calculations from conventional slope stability analyses. On December 8, 1990, Cluer (1992) installed an automatic 35-mm camera to monitor sandbar 172L. The sandbar was photographed every day at 5:00 p.m. corresponding to, approximately, the lowest daily river stage. Image processing of the photographs gave the daily exposed sandbar areas. Typical changes from ground survey data on a cross section in the middle of sandbar 172L are shown in Fig. 5.

From May 22 to May 30, 1991, a research flow with a constant discharge of 426 m<sup>3</sup>/s was released from Glen Canyon Dam. On the initiation of the constant flow, Cluer (1992) measured a constant rate of increase in the area of sandbar 172L. On June 4, 1991, another research flow consisting of 27 days of widely fluctuating discharges was initiated. The discharge fluctuated between 68 and 836 m<sup>3</sup>/s, with a mean of 380 m<sup>3</sup>/s. This series of experimental discharges, called "normal summer" was designed to replicate discharges released during usual summer periods. The minimum and maximum flow, and ramping rates were constrained by dam-management guidelines, but daily range was allowed to fluctuate according to power demands.

During the "normal summer" research-flow regime, deposition occurred at a slower rate than during the period of constant flow. On June 18, 1991, Cluer's (1992) photographs revealed that the sandbar area increased significantly [Fig. 6(a)] and achieved a slope of 26° (ground survey measurements). The profile of the sandbar on June 18, 1991 [Fig. 6(a)] is similar to ground survey measurements made on June 2, as shown in Fig. 5. On June 19, a slope failure of the sandbar was recorded by Cluer's automatic camera. An approximately vertical bank cut traversed the vegetation zone along the length of the sandbar [Fig. 6(b)]. The time when the event took place is unknown (it could have been sometime between 5:00 p.m. on June 18 and 5:00 p.m. on June 19) but it is assumed from prior observations that it may have occurred at the low-river stage (about 5:00 p.m. on June 18). On June 20, with widely fluctuating discharges continuing, deposition resumed but at a much greater rate than before the slope failure. The sandbar grew wider and higher with each daily fluctuation. Slope failures recurred, but since the sandbar grew well into the channel, tractive forces were assumed to play a large role in triggering these failures.

Over 100 sandbar profiles were surveyed before and after each research flow by one or two survey crews (Beus et al. 1992) thus ground surveys only gave geometric changes of a sandbar at a given time. They rarely capture the real sequence of events before, during, and after failures occurred. For

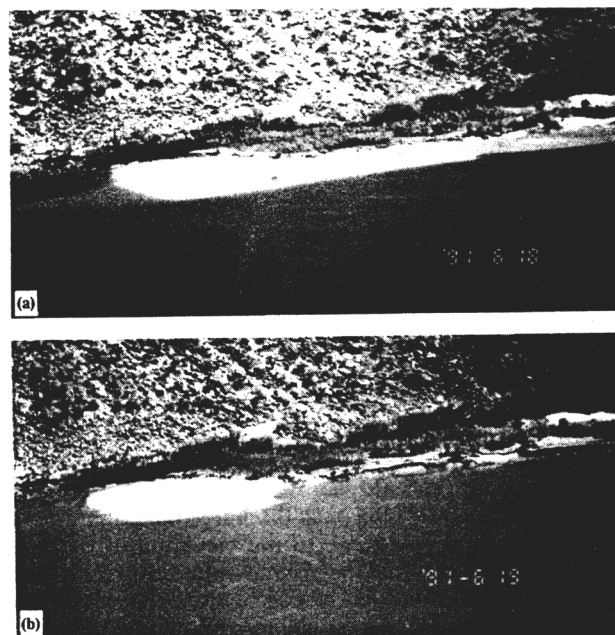


FIG. 6. Sandbar 172L on: (a) June 18, 1991; and (b) June 19, 1991 (Courtesy of B. Cluer)

example, the survey measurements on June 29, 1991 (Fig. 5) can be interpreted as the sandbar profile after a failure occurred some time between June 2, 1991 and June 28, 1991. However, the time-lapsed photographs showed that the sandbar collapsed to the profile ABCD (Fig. 5) on June 18, 1991 and then redeposition resumed. Thus, the survey measurements of June 29, 1991, represent the sandbar in an aggradational mode. During the study period, slope failures on sandbar 172L occurred frequently but never progressed beyond ABCD in Fig. 5.

## SEEPAGE EROSION MODELS

The slope failures observed on sandbar 172L were either triggered by seepage or by tractive forces or a combination. Tractive force appeared to dominate when accretion increased the sandbar well into the main channel. However, most of the observed slope failures were initiated by seepage forces and high pore-water pressures. In the following, we propose two models to predict seepage erosion. One is a simple model intended to provide a quick estimate of the maximum stable seepage slope. The other is a two-dimensional finite-element model that captures the transient loading from river-stage fluctuations to predict when and where failure would occur.

### Simple Model

Taylor (1948) showed that, for a homogeneous, infinite, saturated slope of cohesionless soil with stress-free boundaries, the stable slope angle ( $\beta$ ) under seepage parallel to the slope is

$$\beta = \tan^{-1} \left( \frac{\gamma'}{\gamma_{\text{sat}}} \tan \phi \right) \quad (1)$$

where  $\gamma'$  = effective unit weight;  $\gamma_{\text{sat}}$  = saturated unit weight; and  $\phi$  = angle of friction of the soil. Consider a sandbar at its maximum depositional slope as shown in Fig. 7. As the dam discharge increases to meet power demands, the river stage rises and infiltration into the sandbar occurs. At peak river stage, the ground-water level in the sandbar can be represented by ABC in Fig. 7. If the peak discharge is held

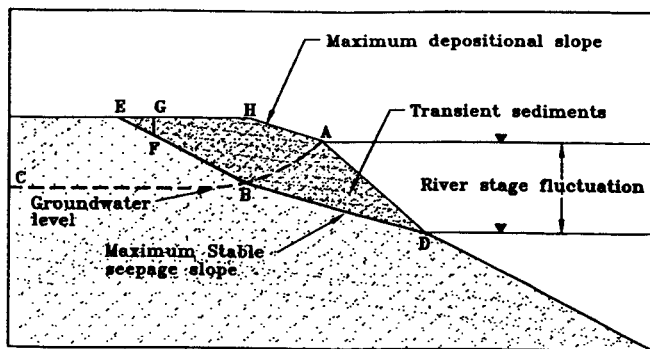


FIG. 7. Determination of Maximum Stable Seepage Slope Using Simple Model

for some time (peak discharge holding time), the groundwater level within the sand will rise with point A remaining fixed. For a sufficiently long peak discharge holding time, the ground-water level would rise to the elevation of the peak river stage. The position of the ground-water level for a given sandbar depends on the rate of rise of river stage, the peak discharge holding time and the soil permeability (Budhu and Gobin 1995). The peak discharge from Glen Canyon Dam is usually maintained for about only 2–4 hr. This peak discharge holding time is too short for the ground water to equilibrate with the river-stage level. Consequently, the soil (sand) mass above the ground-water level is unsaturated except for the capillary zone just above the ground-water level.

In a saturated-unsaturated cohesionless soil, we propose the following procedures to determine the approximate maximum stable seepage slope:

1. The slope angle for a stable slope under seepage, (1), is approximately valid for the lower portion of the seepage face. That is, a line (plane) BD, of slope  $\beta$  drawn from the lowest river stage intersecting the ground-water surface at B represents the maximum lower stable seepage slope (Fig. 7).
2. The stable slope for the portion of the sandbar above the ground-water surface will be the soil's angle of friction ( $\phi$ ) represented by line (plane) BE.
3. If the soil has some cohesion, then a vertical face (tension crack), GF, of depth

$$h_c = 2c/(\gamma\sqrt{K_a}) \quad (2)$$

where  $c$  = cohesion; and  $K_a$  = lateral earth pressure coefficient, will intersect the slope BE at F. The presence of vegetation, in particular tree roots, would increase the depth of the vertical face by reinforcing the soil mass. Capillary action can also cause the formation of vertical faces on sandbars. However, such faces will be unstable when the sandbar is inundated.

The surface DBE or DCFG represents the maximum stable seepage surface (slope) of a saturated-unsaturated sandbar under seepage stresses. The soil enclosed within DCFGHAD or DCFGHAD (Fig. 7) constitutes soil that would be involved in slope failures from ground-water seepage. Generally, the sharp changes at B and F are unlikely and a smooth transition in slopes is to be expected. In this simple analysis, for a given soil the extent of the slope failures increase if: (1) The river stage is lowered through lower dam discharges; and (2) the peak discharge holding time increases or, in the extreme case, is sufficiently long to bring the ground-water level to the same elevation as the river stage (Budhu and Gobin 1995).

The foregoing is a very simple, approximate, procedure to

determine the maximum stable seepage slope for an otherwise complex problem. However, this procedure provides a first approximation to determine the extent of slope instability due to seepage erosion. When and under what conditions slope stability will occur under transient conditions is indeterminate in the simple model.

### Numerical Model for Erosion under Transient Seepage

We formulated a numerical model for erosion under transient seepage using Biot (1941) coupled stress–pore water pressure theory. The ground-water level (free surface) within a sandbar fluctuates with transient river stage. Thus, the effective stresses, consolidation ratio and the permeability of the soil mass can vary with river stage. The advantage of utilizing Biot's theory is that stress changes, pore-water pressures, seepage stresses, slope (bank) stability and the free surface position can be calculated simultaneously.

Biot (1941) presented a coupled theory for consolidation in which pore-water pressures and total stresses are linked by the principle of effective stresses.

$$\sigma'_{ij} = \sigma_{ij} + \delta_{ij}u \quad (3)$$

where  $\sigma'_{ij}$  = total stress;  $\sigma_{ij}$  = effective stress;  $\delta_{ij}$  = Kronecker delta; and  $u$  = pore-water pressure. The equations of equilibrium are

$$\sigma'_{ij}/\partial x_j + B_i = 0 \quad (4)$$

where  $B_i$  = body force unit volume; and  $x_j$  = position of the body. The equation of continuity together with Darcy's law results in

$$\frac{1}{\gamma_w} \left\{ k_x \frac{\partial^2 u}{\partial x^2} + k_y \frac{\partial^2 u}{\partial y^2} + k_z \frac{\partial^2 u}{\partial z^2} \right\} + \frac{\partial \epsilon_v}{\partial t} = 0 \quad (5)$$

where  $k_x, k_y, k_z$  = coefficients of permeability in the  $x, y,$  and  $z$ . Cartesian directions; and  $\gamma_w$  = unit weight of water, which is assumed to remain constant. The volumetric strain  $\epsilon_v$ , is

$$\epsilon_v = \epsilon_1 + \epsilon_2 + \epsilon_3 \quad (6)$$

where  $\epsilon_1, \epsilon_2, \epsilon_3$  = principal strains. In soil mechanics literature, compressive volumetric strains are taken as positive. Eq. (5) can be compared with the conventional equation used in ground-water modeling, that is

$$\left\{ k_x \frac{\partial^2 h}{\partial x^2} + k_y \frac{\partial^2 h}{\partial y^2} + k_z \frac{\partial^2 h}{\partial z^2} \right\} = S \frac{\partial h}{\partial t} \quad (7)$$

where  $h$  = head ( $h = u/\gamma_w$ ); and  $S$  = storativity. Thus, (5) and (7) are identical, provided

$$-\frac{\partial \epsilon_v}{\partial t} = S \frac{\partial h}{\partial t} \quad (8)$$

Under transient flow, the soil can undergo both elastic and plastic volumetric change. Thus, a soil model has to be chosen that would allow the evolution of elastic and plastic strains. There are many models in the literature to select from. The soil model selected is the modified Cam-clay model (Roscoe and Burland 1968) because only a few soil parameters are required to use the model and these can be easily obtained from conventional soil tests.

Let us consider the volume changes from transient changes in ground-water level in a sandbar within the framework of the modified Cam-clay model. The inset diagram in Fig. 8 shows a soil layer with the ground-water level at a distance  $y$  from the ground surface at time,  $t_0$ . The initial state of a typical element,  $X$ , at a distance  $z$  is represented by  $B$  on the void ratio– $\ln(p)$  curve (Fig. 8), as approximated by Schofield

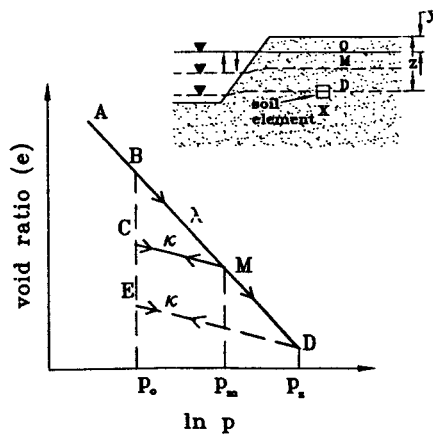


FIG. 8. Void Ratio- $\ln(p)$  Curve

and Wroth (1968). The curve  $AM$  is the loading curve with a slope of  $\lambda$  and  $MC$  is the unloading/reloading curve with a slope of  $\kappa$ . We assumed, for simplicity, that the soil is normally consolidated in its existing state. If it were not, then  $B$  would lie on the curve  $MC$ . Suppose the ground-water surface drops to a new position  $M$ , the mean effective stress on a typical element will increase from, say, an initial value of  $p_0$  to  $p_m$ . The soil consolidates and the total change in void ratio is

$$\Delta e = \lambda \ln(p_m/p_0) \quad (9)$$

and the total change in volumetric strain is

$$\Delta \epsilon_v = \frac{\lambda}{1 + e_0} \ln \frac{p_m}{p_0} \quad (10)$$

where  $e_0$  = initial void ratio. The total change in volumetric strain can be decomposed into two parts, an elastic part,  $\Delta \epsilon_v^e$ , such that

$$\Delta \epsilon_v = \Delta \epsilon_v^e + \Delta \epsilon_v^p \quad (11)$$

If the ground-water level was to rise to its original position, the path followed will not be  $MB$  but  $MC$  (Fig. 8)—the elastic line. The elastic volumetric strain component obtained from the slope of the line  $MC$  is

$$\Delta \epsilon_v^e = \frac{\kappa}{1 + e_0} \ln \frac{p_m}{p_0} \quad (12)$$

where  $\kappa$  = taken as positive for compression, and the plastic component is

$$\Delta \epsilon_v^p = \frac{\lambda - \kappa}{1 + e_0} \ln \frac{p_m}{p_0} \quad (13)$$

Suppose that the ground-water level now drops to the elevation of the soil element (point  $D$ ). The mean effective stress will then increase to a value  $p_z$ , which is greater than the maximum past mean effective stress  $p_m$ . The total change in volumetric strain as a result of this loading condition (path  $CMD$ ) is

$$\Delta \epsilon_v = \frac{1}{1 + e_0} \left[ \kappa \ln \left( \frac{p_m}{p_0} \right) + \lambda \ln \left( \frac{p_z}{p_m} \right) \right] \quad (14)$$

If the ground-water level were to subsequently rise to its original position, the soil stress would follow path  $DE$ . The changes in elastoplastic volumetric strains resulting from transient conditions can now be incorporated into (5). For example, if the ground-water level fluctuations are within the elastic region,  $MC$ , (5) becomes

$$\left( k_x \frac{\partial^2 h}{\partial x^2} + k_y \frac{\partial^2 h}{\partial y^2} + k_z \frac{\partial^2 h}{\partial z^2} \right) = \frac{\kappa}{\rho_0(1 + e_0)} \frac{\partial p_0}{\partial t} \quad (15)$$

and if the past maximum mean effective stress is exceeded, the governing elastoplastic equation is

$$\left( k_x \frac{\partial^2 h}{\partial x^2} + k_y \frac{\partial^2 h}{\partial y^2} + k_z \frac{\partial^2 h}{\partial z^2} \right) = \frac{1}{1 + e_0} \left( \frac{\kappa}{\rho_0} \frac{\partial p_0}{\partial t} - \frac{\lambda}{p_z} \frac{\partial p_z}{\partial t} \right) \quad (16)$$

The soil parameters  $\kappa$  and  $\lambda$  can be found by conducting a consolidation test on the soil and finding the slopes of the loading and unloading lines. If the changes in stress from ground-water level fluctuations lie within the unloading/reloading line then the soil is overconsolidated and an elastic analysis can be used as an approximation (Wroth 1971). In this case,  $\kappa$  can be found from the shear modulus ( $G$ ) of the soil through the relationship (Wroth 1971)

$$\kappa = \frac{1.5p(1 + e_0)(1 - 2\mu)}{(1 + \mu)G} \quad (17)$$

where  $p$  = mean effective stress; and  $\mu$  = Poisson's ratio. The solution for (5), over the whole domain, is found using standard numerical techniques [for example, Smith and Griffiths (1988)].

### GROUND-WATER LEVEL VARIATIONS FROM TRANSIENT DAM FLOW

One of the first tasks in modeling seepage erosion is to predict the changes in ground-water level during transient flow. Biot's (1941) coupled stress-pore water pressure equation was solved using a fixed-mesh finite-element procedure (Desai 1976; Bathe and Khoshgoftaar 1979; Desai and Li 1983; Desai 1984; Lacy and Prevost 1987; Cividini and Giada 1989). In the fixed-mesh procedure, the mesh is kept constant and the whole domain (saturated and unsaturated zones) is discretized. The location of the ground-water level (free surface) is found by interpolating between positive and negative pressure heads. The following procedures were followed:

1. The pore-water pressures for the soil domain above the ground-water level were initially set to zero.
2. The permeability of the soil in the unsaturated domain was assumed to be approximately 1/1,000 of the permeability of the saturated domain (Bathe and Khoshgoftaar 1979).
3. The location of the ground-water surface was found by interpolating between the negative pore-water pressures computed for the soil domain above the ground-water surface and the positive pore-water pressures computed for the saturated region (Li and Desai 1983; Desai 1984).

The prediction of the numerical analysis developed here is evaluated by comparison with a set of ground-water data collected along sandbar 172L. We will only use an arbitrarily selected portion of the ground-water data to validate the numerical analysis for free surface determination under transient flow conditions. The cross section shown in Fig. 4 was discretized into 312 isoparametric quadrilateral elements and hydrostatic stresses were imposed on the face of the slope following the rate of rise and fall of the river stage. The stage measurements and ground-water level (well #63, Fig. 4) recorded over a 4-day period (June 12 to June 16) are shown in Fig. 9. For brevity, we will only present the results for June 14. Hydrostatic stress was imposed on the slope following the river-stage variation, which was approximated as shown in the inset figure in Fig. 10. The soil parameters used in the model are shown in Table 1. The results of the free-surface prediction from the finite-element model are compared with

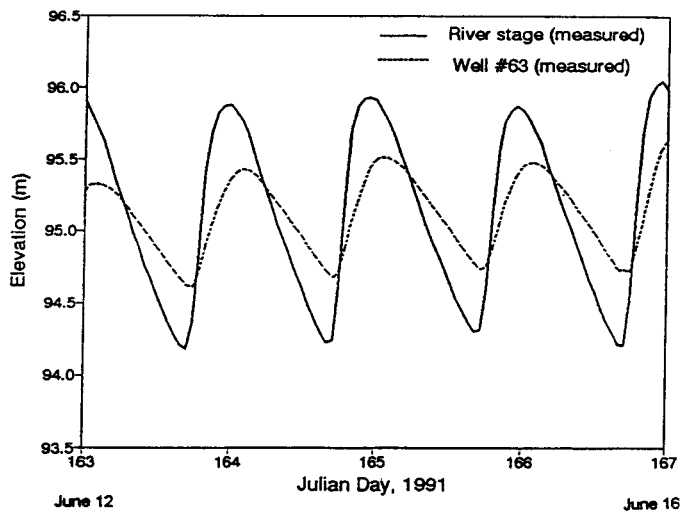


FIG. 9. River Stage and Ground-Water Level Variation in Well #63 from June 12 to June 16, 1991

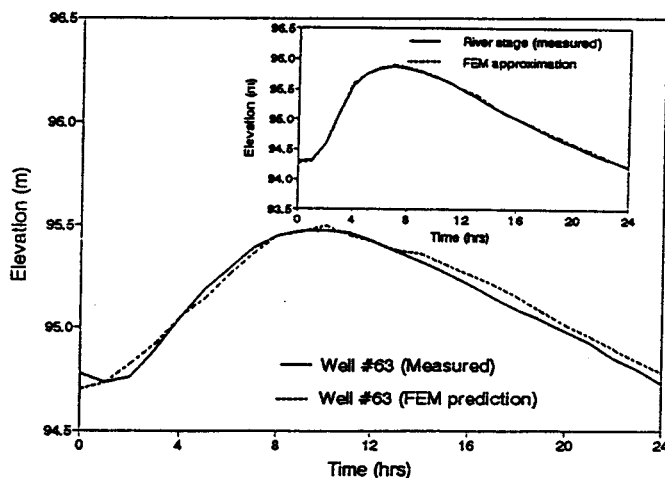


FIG. 10. Comparison between Finite-Element Prediction of Ground-Water and Well #63 on June 14, 1991

field measurements in Fig. 10. The predicted free surface is in accord with the field measurements. Similar good agreement between the finite-element predictions and field measurements of the free surface under different flow regimes was obtained for other sandbars in the Grand Canyon.

#### COMPARISON OF SIMPLE MODEL WITH FIELD DATA

The simple model is intended to establish the maximum stable seepage slope below which slope failures would not occur from ground-water seepage. The input data required to use the simple model are: (1) The current sandbar profile; (2) the elevation of the lowest river stage; (3) the location of the ground-water surface; and (4) the unit weight and friction angle of the soil. The average maximum depositional slope for the sandbars in the Grand Canyon recorded during the research flows was  $\approx 26^\circ$ . The lowest river-stage elevation was 92.6 m.

The predicted ground-water surface for sandbar 172L, under a peak dam discharge of 836 m<sup>3</sup>/s, from the finite-element solution of Biot's equation is shown in Fig. 11. The lower stable seepage slope (BD, Fig. 7) from (1) is  $12.6^\circ$  ( $\gamma_{sat} = 16$  kN/m<sup>3</sup> and  $\phi = 30^\circ$ ) and the upper stable seepage slope (BE, Fig. 7) is  $30^\circ$ . The predicted stable seepage slope is in accord with the stable profile measured on July 14, 1991 (Fig. 11). Similar agreement was obtained using this simple model for other sandbars in the Grand Canyon (Budhu and Gobin 1994).

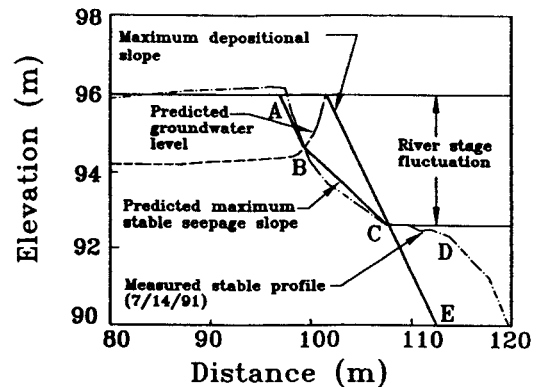


FIG. 11. Comparison of Maximum Stable Seepage Slope Predicted by Simple Model with Field Data for Sandbar 172L

#### COMPARISON OF FINITE-ELEMENT MODEL PREDICTIONS WITH FIELD DATA

The finite-element model was used to predict the failure event captured by time-lapsed photography (Cluer 1992) on June 18, 1991, at sandbar 172L. The profile of sandbar 172L measured on June 2, 1991 was discretized into 312 isoparametric quadrilateral elements, and the following procedure was followed in the finite-element algorithm:

1. Sandbar 172L was subjected to a river stage higher than that during the research-flow period. Accordingly, the soil was assumed to be elastic lying on path *MC* (Fig. 8).
2. Hydrostatic stresses were imposed on the face of the slope following the rise and fall of the river stage as measured on June 18.
3. The effective unit weight ( $\gamma'$ ) of the soil was reduced or increased by the seepage force per unit volume ( $j$ ) depending on the direction of the seepage vector. If the seepage vector was upward directed, the effective unit weight was reduced to  $\gamma'_c = \gamma' - j'$ ; whereas if the seepage vector was downward directed, the effective unit weight was increased to  $\gamma'_c = \gamma' + j'$ , where  $\gamma'_c$  is the current effective unit weight and  $j'$  is the vertical component of the seepage vector. The corresponding upward or downward forces were computed for each element and used as nodal forces.
4. Failure was governed by Mohr-Coulomb failure criterion.
5. A check was made at each Gaussian point (nine in the isoparametric quadrilateral elements used in the algorithm) to determine whether the failure state is reached or the mean effective stress approaches zero. In the former case, the Gaussian points were flagged to delineate the failure surface. Each Gaussian point was taken to represent 1/9 of the area of the element. For the latter case, the element was removed (eroded element) when at least eight of the nine Gaussian points showed that the mean effective stress was near to zero. In preliminary numerical tests, we found that there was a reduction in computational time if the stiffness of the eroded element was reduced by at least 1/1,000 of its original value leaving the element in the mesh instead of removing it and increasing the soil permeability by 100 times. There was no significant practical difference ( $<5\%$ ) between the results from reducing the stiffness and leaving the mesh intact, and removing the element and reforming the mesh.

It was observed during the study period that slope failures

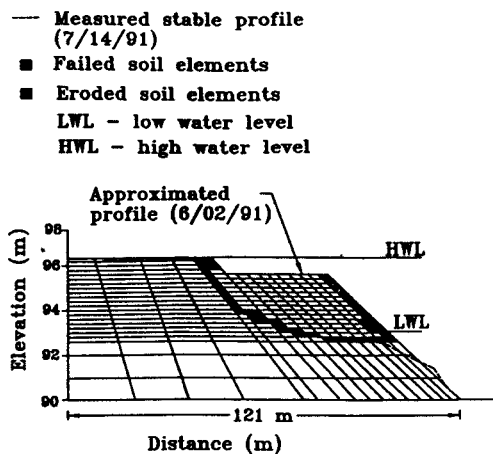


FIG. 12. Finite-Element Prediction of Failure Zone when Interface Elements are Included

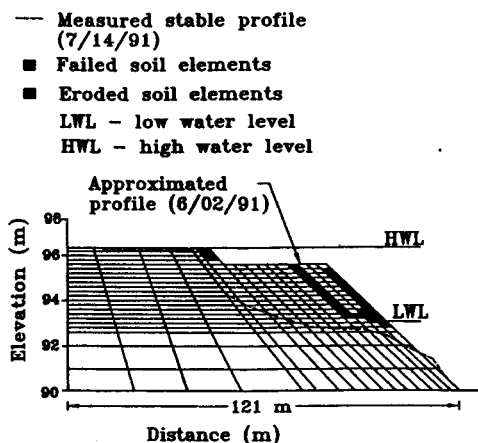


FIG. 13. Finite-Element Prediction of Failure Zone without Interface Element

on sandbar 172L only regressed as far as ABCD (Fig. 5). This line delineated the two distinct material zones. For the finite-element model, an interface approximately following the line ABCD (Fig. 5) was introduced between these two zones. The soil properties assumed for the interface is the same as for zone I but with cohesion taken as zero. The predicted failure zone at the end of the stage variation is shown in Fig. 12. Comparison between this failure plane and the measured failure show good agreement (Fig. 12). One would expect that, if failure was to occur, the discontinuity between the deposits would be the likely location for the failure surface. The introduction of an interface in the numerical model practically predefines the failure surface. Thus, the agreement between the predicted and measured failure plane is not surprising. What would be the result if an interface was not used? We repeated the analysis by removing the interface and used the soil properties for the two zones, as shown in Table 1. The results of this analysis showed a shallow slope failure (Fig. 13), which did not agree with field observations and measurements.

Elements close to the sandbar face are subjected to large hydraulic gradients. Consider a slope,  $\alpha$ , and a surface of seepage AB, in which the seepage vector exit the slope at an angle  $\theta$  to an outwardly directed normal to the slope (Fig. 14). Harr (1962) showed that at the discharge point B, the hydraulic gradient  $i \rightarrow \infty$ , that is, the hydraulic gradient is unbounded and Darcy's law is not valid. However, in practice this would not occur (Harr 1962), but the hydraulic gradient would be sufficiently large to cause static liquefaction of the

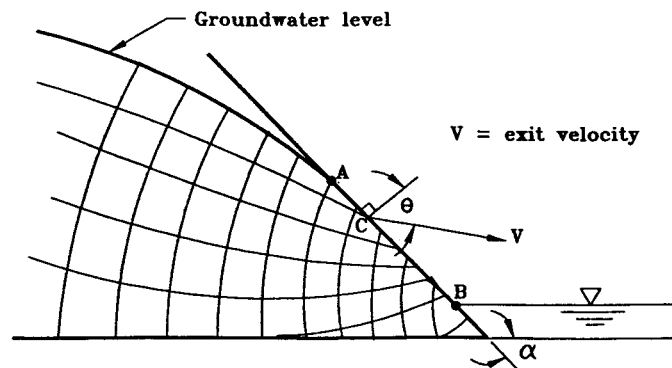


FIG. 14. Direction of Seepage Vector along Seepage Surface

TABLE 2. Results from Conventional Stability Analyses

Method of analysis (1)	Factor of Safety	
	RD1 (2)	RD2 (3)
Spencer (1967)	4.15	1.75
Janbu (1954)	4.18	1.60
USACE-modified Swedish (1970)	4.10	1.72
Lowe and Karafiath (1960)	3.90	1.70

sand. Static liquefaction is identified in our algorithm when the mean effective stress in an element approaches zero. Elements of soil that have statically liquefied would flow out of the sandbar. The sand mass just above the cavity created by the outflow of the sand usually collapsed into the cavity as was observed on sandbars in the Grand Canyon. The elements of sand that have statically liquefied prior to the slope failure on sandbar 172L are shown by the hatched areas in Figs. 12 and 13. All these elements are on or near the face of the sandbar where the hydraulic gradients are expected to be large enough to cause static liquefaction.

#### COMPARISON OF CONVENTIONAL STABILITY ANALYSES WITH FIELD DATA

We used a few conventional slope-stability analyses to examine the factor of safety of sandbar 172L under two conditions.

- RD1—a rapid drawdown condition using the groundwater surface as measured in the field (Carpenter 1992) at peak river stage and the external water level at elevation 92.6 m (low-water level).
- RD2—a rapid drawdown condition with the groundwater level at the same elevation as the peak river stage and the external water level at elevation 92.6 m (low-water level)—worst-case conditions.

We used stability analyses that utilized a noncircular failure surface and specified the observed failure surface (discontinuity between zone I and zone II soil) as the failure surface for which a factor of safety is being sought. The results are summarized in Table 2. As expected, the factors of safety for RD2 are much lower than RD1 because of the higher pore-water pressures in RD2. The conditions imposed by RD2 are unusual because the duration of the peak was too short for the groundwater level to rise to the river-stage elevation.

It is known that although these conventional slope stability analyses are based on the same fundamental principles, they give different results for the factor of safety mainly because of the differences in interslice forces (Whitman and Bailey 1967). Further review of some of these methods by Duncan

et al. (1990) showed that differences could come from different representation of the soil strength. None of the conventional analyses examined here predicted failure. We repeated these analyses without specifying a failure surface; all predicted shallow slope failures similar to the finite-element analyses are shown in Fig. 13. The disagreement is not surprising since: (1) The interface at the two soil zones is a discontinuity and becomes a preferred failure plane; and (2) the condition under which slope failures occur in the Grand Canyon is different from the classical undrained failures under rapid drawdown where high pore pressures are responsible for failures.

## CONCLUSIONS

For sandbars where instability is caused by outward groundwater seepage, there is a maximum stable seepage slope below which slope failures would be unlikely. Sands deposited between this maximum stable seepage slope and the maximum depositional slope angle will undergo cyclic aggradation and erosion depending on the dam discharge regimes. The maximum stable seepage slope defines a preferred failure surface for freshly deposited sediments subjected to outwardly directed seepage forces.

The simple model described in this paper can be used as a first approximation to delineate the maximum stable seepage surface. The finite-element analyses using Biot's equations provided predictions that were in accord with field observations only when an interface was included. None of the conventional slope analyses examined predicted failure for the observed failure zone of material.

Evaluation of the models and the field observations suggests that for a given set of dam discharge regimes, sandbars would acquire an equilibrium profile (maximum stable seepage slope). If the dam operation were to change, the river system including the sandbars would be reworked to a new equilibrium position consistent with the new discharge regimes. In particular, lower river stage and longer peak-discharge holding time would result in larger slope failures. Slope failures in sandbars in the Grand Canyon involve transient sediments deposited under favorable hydraulic and hydrological conditions.

## ACKNOWLEDGMENTS

The writers thank the Glen Canyon Environmental Studies (GCES) for the financial support of this research. The ground-survey data was supplied to us by Prof. S. Beus and M. Kaplinski, of Northern Arizona University. Dr. M. Carpenter and Rob Carruth, of the U.S. Geological Survey, provided the information to generate the soil profile, ground water and river stage for sandbar 172L. B. Cluer, of the GCES, provided details of failures captured by time-lapsed photography. We thank these scientists for the information provided and Drs. L. Stevens and D. Wegmer from the GCES. This paper does not necessarily reflect the views of the GCES group.

## APPENDIX I. REFERENCES

- Bathe, K. J., and Khoshgoftaar, M. R. (1979). "Finite element free surface seepage analysis without mesh iteration." *Int. J. Num. Anal. Methods Geomech.*, Vol. 3, 13-22.
- Biot, M. A. (1941). "Theory of elasticity and three dimensional consolidation." *J. Appl. Physics*, Vol. 12, 155-164.
- Budhu, M. (1992). "Mechanisms of erosion and a model to predict seepage due to transient flow." *The influence of variable discharge on Colorado River sandbars below Glen Canyon Dam: final rep. to the National Park Service*, S. S. Beus and C. C. Avery, eds., Flagstaff, Ariz.
- Budhu, M., and Gobin, R. (1994). "Instability of sandbars in Grand Canyon." *J. Hydr. Engrg.*, ASCE, 120(8), 919-932.
- Budhu, M., and Gobin, R. (1995). "Seepage erosion from dam-regulated flow: case of Glen Canyon Dam, Arizona." *J. Irrig. Engrg.*, ASCE, 121(1), 22-23.
- Carpenter, M. C., Carruth, R. L., Fink, J. B., Boling, J. K., and Cluer, B. L. (1992). "Hydrogeology of beaches 43.1L and 172.3L and the implications of flow alternatives along the Colorado River in the Grand Canyon." *The influence of variable discharge on Colorado River sandbars below Glen Canyon Dam: final rep. to the National Park Service*, S. S. Beus and C. C. Avery, eds., Flagstaff, Ariz.
- Cividini, A., and Gioda, G. (1989). "On the variable mesh finite element analysis of unconfined seepage problems." *Géotechnique*, London, England, (2), 251-267.
- Cluer, B. L. (1992). "Daily response of Colorado River sandbars to Glen Canyon Dam test flows, Grand Canyon, Arizona, and analysis of sandbar response along the Colorado River in Glen and Grand Canyon to test flows from Glen Canyon Dam, using aerial photographs." *The influence of variable discharge on Colorado River sandbars below Glen Canyon Dam: final rep. to the National Park Service*, S. S. Beus and C. C. Avery, eds., Flagstaff, Ariz.
- Corps of Engrs. (1970). "Engineering and design—stability of earth and rock-fill dams." *Engr. Manual EM 1110-1902*, Dept. of the Army, Ofc. of the Chf. Engr., Washington, D.C.
- Desai, C. S. (1976). "Finite element residual schemes for unconfined flow." *Int. J. Num. Methods in Engrg.*, Vol. 5, 1415-1418.
- Desai, C. S. (1984). "Chapter 18: free surface flow through porous media using a residual procedure." *Finite elements in fluids*, 5, R. H. Gallagher, J. T. Oden, O. C. Zienkiewicz, T. Kawai, and M. Hawahara, eds., Wiley & Sons, Inc., New York, N.Y.
- Desai, C. S., and Li, G. C. (1983). "A residual flow procedure and application for free flow in porous media." *Advances in Water Resour.*, Vol. 6, 27-35.
- Duncan, M., Wright, S., and Wong, K. S. (1990). "Slope stability during rapid drawdown." *Proc., H. Bolton Seed Memorial Symp.*, J. Michael Duncan, ed., BiTech Publishers Ltd., Vancouver, B.C., Canada, Vol. 2, 253-271.
- Harr, M. E. (1962). *Groundwater and seepage*. McGraw-Hill, New York, N.Y.
- Howard, A. D., and McLane, C. F. III. (1988). "Erosion of cohesionless sediment by groundwater seepage." *Water Resour. Res.*, 24(10), 1659-1674.
- The influence of variable discharge on Colorado River sandbars below Glen Canyon Dam: final rep. to the National Park Service*. (1992). S. S. Beus and C. C. Avery, eds., Flagstaff, Ariz.
- Janbu, N. (1954). "Application of composite slip surface for stability analysis." *Proc., European Conf. on Stability of Earth Slopes*, Statens Reproduktionsanstalt, Stockholm, Sweden, Vol. 3, 43-49.
- Lacy, S. J., and Prevost, J. H. (1987). "Flow through porous media: a procedure for locating the free surface." *Int. J. Num. Anal. Methods Geomech.*, 11(6), 585-601.
- Li, G. C., and Desai, C. S. (1983). "Stress and seepage analysis of earth dams." *J. Geotech. Engrg.*, ASCE, 109(7), 946-960.
- Lowe, J. III, and Karafiath, L. (1960). "Stability of earth dams upon drawdown." *Proc., 1st Panamerican Conf. on Soil Mech. and Found. Engrg.*, Mexico City, Mexico, Vol. 2, 537-552.
- Roscoe, K. H., and Burland, J. B. (1968). "On the generalised stress-strain behaviour of a wet clay." *Engineering plasticity*, J. Heyman and F. A. Lechic, eds., Cambridge University Press, Cambridge, England, 535-609.
- Schmidt, J. C., and Graf, J. B. (1990). "Aggradation and degradation of alluvial sand deposits 1965 to 1986, Colorado River, Grand Canyon National Park, Arizona." *Paper 1493*, U.S. Geological Survey, Washington, D.C.
- Schofield, A. N., and Wroth, C. P. (1968). *Critical state soil mechanics*. McGraw-Hill Book Co., London, England.
- Smith, I. M., and Griffith, D. V. (1988). *Programming the finite element method*. Wiley and Sons, Inc., New York, N.Y.
- Spencer, E. (1967). "A method of analysis of the stability of embankments assuming parallel inter-slice forces." *Géotechnique*, London, England, 17(1), 11-26.
- Taylor, D. W. (1948). *Fundamentals of soil mechanics*. John Wiley and Sons, New York, N.Y.
- Werrell, M., Inglis, R. Jr., and Martin, L. (1992). "Erosion of sand bar 43.1L along the Colorado River in Grand Canyon in response to groundwater seepage during fluctuating flow releases from Glen Canyon Dam." *The influence of variable discharge on Colorado River sand bars below Glen Canyon Dam: final rep. to the National Park Service*, S. S. Beus and C. C. Avery, eds., Flagstaff, Ariz.
- Whitman, R. V., and Bailey, W. A. (1967). "Use of computers for slope stability analysis." *J. Soil Mech. and Found. Div.*, ASCE, 93(4), 475-497.
- Wroth, C. P. (1971). "Some aspects of the elastic behavior of overconsolidated clay." *Proc., Roscoe Memorial Symp.*, Foulis, 347-361.

## APPENDIX II. NOTATION

The following symbols are used in this paper:

$B_v$  = body force per unit volume;  
 $c$  = cohesion;  
 $e$  = void ratio;  
 $e_0$  = initial void ratio;  
 $G$  = shear modulus;  
 $h$  = head;  
 $h_c$  = depth of tension crack;  
 $j$  = seepage force per unit volume;  
 $K_a$  = coefficient of lateral active earth pressure;  
 $k_x, k_y, k_z$  = coefficient of permeability in the  $x$ ,  $y$ , and  $z$  Cartesian directions;  
 $p$  = effective stress;  
 $S$  = storativity;  
 $t$  = time;  
 $u$  = pore-water pressure;  
 $x$  = position of the body;

$x, y, z$  = Cartesian coordinate directions;  
 $\alpha$  = slope angle;  
 $\beta$  = stable seepage slope;  
 $\gamma$  = bulk unit weight;  
 $\gamma'$  = effective unit weight;  
 $\gamma_{\text{sat}}$  = saturated unit weight;  
 $\gamma_w$  = unit weight of water;  
 $\delta_{ij}$  = Kronecker delta;  
 $\epsilon_e^p$  = plastic volumetric strain;  
 $\epsilon_v$  = volumetric strain;  
 $\epsilon_v^e$  = elastic volumetric strain;  
 $\epsilon_1, \epsilon_2, \epsilon_3$  = principal strains;  
 $\theta$  = inclination of exit seepage vector with outward normal to slope;  
 $\kappa$  = slope of unloading/reloading curve;  
 $\lambda$  = slope of loading curve;  
 $\mu$  = Poisson's ratio;  
 $\sigma_{ij}$  = effective stress;  
 $\sigma'_{ij}$  = total stress; and  
 $\phi$  = angle of friction.